J Mater Sci (2007) 42:428–443
DOI 10.1007/s10853-006-0873-2

The hydration of slag, part 1: reaction models for alkali-activated slag

W. Chen · H. J. H. Brouwers

Received: 10 February 2005 / Accepted: 22 December 2005 / Published online: 29 November 2006

Abstract Reaction models are proposed to quantify the hydration products and to determine the composition of C–S–H from alkali-activated slags (AAS). Products of the slag hydration are first summarized from observations in literature. The main hydration products include C–S–H, hydrotalcite, hydrogarnet, AFm phases (C_4AH_{13} and C_2ASH_8) and ettringite. Then, three stoichiometric reaction models are established correlating the mineral composition of slag (the glass part) with the hydration products. Using the proposed models, quantities of hydration products and composition of C–S–H are determined. The models are validated with a number of experimental investigations reported in literature, yielding good agreement, i.e., these models can successfully predict the hydration reaction of AAS. The models are furthermore applied to calculate the retained water in the hydration products of AAS in different hydration states and a general hydration equation of AAS is derived. As an illustration to one of the model applications, chemical shrinkage of the AAS cement paste in different hydration states are predicted. The chemical shrinkage of AAS is shown to be remarkably higher than OPC. Furthermore, phase distribution in the hardened AAS paste and the porosity are calculated.

W. Chen · H. J. H. Brouwers (✉)
Construction Management & Engineering, Department of Civil Engineering, Faculty of Engineering Technology, University of Twente, P.O. Box 217, Enschede 7500 AE, The Netherlands
e-mail: H.J.H.Brouwers@ctw.utwente.nl

List of symbols

Oxides

A	Al_2O_3
S	SiO_2
C	CaO
F	Fe_2O_3
M	MgO
$\overline{S}$	SO_3
H	H_2O

Abbreviations

AAS	Alkali-activated slag
A/C	A/C molar ratio in C–S–H
BSE	Backscattered electron
EMPA	Electron microprobe analysis
EDX	Energy-dispersive X-ray
GGBFS	Ground granulated blast-furnace slag
M	Molar mass of substance (g/mole)
NMR	Nuclear magnetic resonance
OPC	Ordinary Portland cement
SEM	Scanning electron microscopy
S/C	S/C molar ratio in C–S–H
TEM	Transmission electron microscopy
XRD	X-ray diffraction
a	C/S ratio in C–S–H
b	A/S ratio in C–S–H
m	Mass of substance
n	Moles of substance
w/b	Water/binder ratio in mass
x	Mass fraction of constituent in slag
y	Mole content of constituent in slag (mole/g)

Greeks

Φ	Porosity
Ψ_S	Chemical shrinkage
ρ	Density (g/cm^3)
ρ_0	Density of the initial paste (g/cm^3)
ω	Molar volume (cm^3/mole)

Subscripts

AH	Tetracalcium aluminate hydrate
AFt	Ettringite
C–S–H	Calcium silicate hydrate
CH	Calcium hydroxide
HT	Hydrotalcite
HG	Hydrogarnet
H	The retained water in hydration products
ST	Strätlingite
hp	Hydration product
cp	Capillary porosity
gp	Gel porosity
sl	Slag
w	Water
w_0	Water in the initial paste
x	H/S ratio in the C–S–H

Introduction

Researches on the alkali-activated slag (AAS) grew remarkably in the recent decades because of its numerous advantages such as fast development of strength, high resistance to chemical attack, and low heat release, if compared to normal Portland cement [1]. Furthermore, since the slag is an industrial by-product, use of AAS has many environmental advantages such as low energy cost, use of secondary raw material and low pollutant gas emission. These advantages make it preferable to conventional binders in practice.

The commonly used alkali activators in AAS are sulfate, Portland cement, sodium silicate and sodium hydroxide. Typical AAS consists of ground granulated blastfurnace slag (GGBFS) with 3.5%–5.5% (in mass) of Na_2O added, usually as sodium hydroxide (NaOH) or water-glass. Increasing the dosage of activators accelerates the strength development and increases the 28d strength of the paste [2].

There are already many researches about analyzing the hydration products of slag and to characterize the hardened AAS paste [2–7]. The main hydration product from the activated slag is a low-basic calcium silicate hydrate (C–S–H). The other hydration products differ slightly due to the differences in the slag compositions, curing time, temperature, and the activator.

Although there are numerous researches on the hydration of AAS, to the authors' knowledge, the reaction mechanism of AAS is not fully understood and the chemistry of slag reaction in AAS remains unclear until now. The lack of knowledge on the hydration of slag obstructs the further application of AAS. Modeling the hydration of the AAS will bring conceivable opportunities for evaluating the potential of reactants and predicting the performance of the hardened AAS paste without the need of time-consuming and costly experiments.

In this study, reaction models are proposed for AAS, which can quantify the hydration products and determine their compositions. Together with the physical properties of the hydration products, the models can predict some properties of the hydrating AAS, such as the chemical shrinkage evolvement, strength development, and waste binding capability. These properties are important when exploring new applications of AAS. Models established in this study are validated with a number of experiments on AAS selected from literature. The models are further applied to calculate the water retention by the hydration products of AAS and sequentially to derive its hydration equation. Chemical shrinkage of the AAS paste in different hydration states is predicted. The phase distribution on a volume basis in the hardened AAS paste is calculated. In Part II of this research, reaction models for the slag blended cement are proposed using models developed in this study [8].

Hydration products

As observed in most experiments, a hydrated calcium silicates gel, namely C–S–H, is the most abundant product in hardened AAS pastes. The C/S ratio (in moles, notation in cement chemistry is used, such as C = CaO, S = SiO_2, A = Al_2O_3, M = MgO, $\bar{S}$ = SO_3, and H = H_2O) in C–S–H is generally close to that of the unhydrated slag. It is much lower than the C/S ratio in C–S–H from the normal Portland cement hydration. C–S–H in AAS paste is highly amorphous and closely mixed with other phases. It is characterized by its high aluminum content. The A/S ratio in it can be as high as 0.1, indicating a high degree of aluminum substitution for silicon in its structure.

Richardson et al. [9] found linear increase of A/C ratios with S/C ratios in single-phase C–S–H. A general model was proposed for the structure of the substituted C–S–H, in which aluminum substitutes for silicon in the bridging tetrahedral of a dreierkette structure. This model was later confirmed by Wang and Scrivener [10] using NMR technique. In a more recent work of Richardson [11], based on the observations in a serial of slag blended cement pastes, a general relationship for the A/C and S/C ratios in the C–S–H was proposed as:

$$S/C = 0.4277 + 4.732\ A/C. \quad (1)$$

Furthermore, an M–A rich phase is commonly found in both AAS and the slag blended cement pastes, generally referred to as the natural mineral hydrotalcite ($M_6A\bar{C}H_{12}$). The hydrotalcite is intimately mixed with C–S–H, making it hard to discern. The M/A ratio in it varies from 3.8 to 8.7 [12]. Harrisson et al. [13] found a phase with an M/A ratio of 5.3 in the slag blended cement paste and deduced it as a member of the hydrotalcite family. Richardson and Groves [14] found an M–A rich phases as part of the ''inner product'' and envisaged it a hydrotalcite phase with an M/A ratio of 4.8. With X-ray microanalysis, Wang and Scrivener [5] found a hydrotalcite phase with an M/A ratio of 4.4 dispersed through the C–S–H. In the study of Gollop and Taylor [15], an M/A ratio of 4 in the hydrotalcite was found in the hardened slag blended cement paste. Allmann [27] derived a layer ions structure by introducing trivalent ions into brucite-like layers with water molecules and a balancing anion in the interlayer sites. Specifically for the hydrotalcite phases, the structure can be attained based on layers of the type $[Mg_{1-x}Al_x(OH)_2]^{x-}$, where '$x$' ranges between 0.2 and 0.4. The balancing anion can be OH^-, Cl^- or CO_3^{2-}, etc. In the same literature, several M/A ratios of hydrotalcite observed in researches were included, ranging from 4 to 6.

X-ray and DTA evidences indicate that there are some AFm phases existing in the paste. They are identified as the tetracalcium aluminate hydrate (C_4AH_{13}) [5] or strätlingite (C_2ASH_8) [9] or both [2, 4] whereas in some AAS pastes neither is found [14]. The tetracalcium aluminum hydrate is most likely formed from glasses rich in lime and poor in alumina [16]. Strätlingite is formed primarily from glasses rich in aluminum or poor in magnesium.

If gypsum is added as activator, commonly together with calcium hydroxide (CH), ettringite is found in AAS pastes while no trace of monosulfate is detected [2]. Gollop and Taylor [17] studied hardened pastes of five slag blended cements with different mass proportions of slag and Portland cement. Ettringite was found in all samples. Monosulfate was observed in four blends at 1 week, while with increasing age its amount decreased. The reason for the decrease can be that monosulfate is easily carbonated in the presence of CO_3^{2-}, Ca^{2+} and OH^- to form ettringite and hemicarbonate or finally mono-carbonate [18–20]. Therefore, in this study, ettringite is taken as the only sulfate-containing hydration product from the slag.

Poorly crystalline particles rich in iron and aluminum are found in AAS pastes, possibly being a form of calcium-deficient hydrogarnet [14]. According to the researches on normal Portland cement and fly ash [21–23], iron oxide in slags probably reacts into a hydrogarnet phase with the approximate composition $C_6AFS_2H_8$. CH in significant amount is rarely detected in AAS pastes. Even if it is formed with some slag high in C, it may react further with C–S–H to increase its C/S ratio or with A to form the AFm phases from a long term point of view.

Summarizing, the main hydration products in mature AAS pastes comprise of C–S–H, hydrotalcite, an Fe rich hydrogarnet phase, ettringite and AFm phases (C_4AH_{13} or C_2ASH_8). Since the reported M/A ratio in the hydrotalcite varies in a wide range, in this study, an M/A ratio of five is assumed. This value is proposed by Taylor [12] and is also close to those measured in experiments [5, 13, 14]. Therefore, the main hydration products of AAS include C–S–H, M_5AH_{13}, $C_6AFS_2H_8$, $C_6A\bar{S}_3H_{32}$, C_4AH_{13} and C_2ASH_8. The formula of C–S–H is denoted as $C_aSA_bH_x$ in which 'a', 'b' and 'x' are the C/S, A/S and H/S ratios in the C–S–H, respectively.

The actual amount of retained water in the hydration products depends on the hydration state of the paste [12, 23]. The hydration state is the drying condition that the paste is subject to, such as the temperature and relative humidity (RH). C–S–H in AAS pastes has a lower C/S ratio than that in OPC pastes. The water level in such C–S–H is not sufficiently investigated. The amount of ''non-evaporable'' water is commonly used as an empirical measurement for the degree of hydration. It is the retained water by the hydration products after the D-drying procedure (equilibrated with dry ice at – 79 °C). Heating the paste to a constant mass at 105 °C in an atmosphere of uncontrolled humidity, but free of CO_2, reduces the retained water to the same extent [12]. In this study, the retained water in the AAS paste after being dried at 105 °C is taken as the non-evaporable water since practically this drying procedure is easier to carry out and researches following it are better documented. For C–S–H with low C/S ratios (1.0–1.1), H/S ratios

between 1 and 1.33 were measured after oven-heating to 105 °C [24]. In this study, this value is fixed as 1.2. Based on the work of Brouwers [18, 19, 25], at 80% RH, the H/S ratio in C–S–H can be expressed with $x = a + 0.8$ and in the saturated state, the H/S ratio $x = a + 1.5$.

At room temperature, if the relative humility keeps higher than 88%, a hydrous form of the tetracalcium aluminum hydrate exists as C_4AH_{19}; at lower relative humility its stable form is C_4AH_{13}; at 22% RH the stable form reverts to C_4AH_{12} and at 11% RH to C_4AH_{11}; if dried at room temperature (25 °C) over P_2O_5 or heated to 120 °C, it turns into C_4AH_7 [23]. At 80% RH, the stable form of ettringite was $C_6A\bar{S}_3H_{32}$ [12], and if further heated to 100 °C, a lower hydrate, namely $C_6A\bar{S}_3H_8$, is formed [26]. Water molecules in the interlayer sites of the hydrotalcite-like phase can be removed reversibly without destroying its double layer structure [27]. So, the water retention capability of the hydrotalcite can also depend on the hydration state. The hydrotalcite has similar layer thickness to that of the AFm phases, so it may also have the same dehydration characterizations as them. In this study, the hydrotalcite is assumed to have the same dehydration characterizations as the tetracalcium aluminate hydrate. At room temperature and at 35% RH, a stable form of the strätlingite (C_2ASH_8) exists [12].

Although the retained water in the hydration products might change in different hydration states and consequently their chemical formulas are changed, the expression $C_aSA_bH_x$, M_5AH_{13}, $C_6AFS_2H_8$, $C_6A\bar{S}_3H_{32}$, C_4AH_{13} and C_2ASH_8 are always used to denote the hydration product C–S–H, hydrotalcite, hydrogarnet, ettringite, tetracalcium aluminate hydrate and strätlingite for simplifying expression purpose. Their different water content will be accounted for when discussing the water retention by the hydration products and calculating the chemical shrinkage.

Reaction models

GGBFS often contains more than 95% glass while some crystalline phases may exist in minor level. Only the glass part in the slag has the latent hydraulic property. The crystalline phases remain intact during the hydration [3]. The main crystalline phases in slags are merwinite (C_3MS_2) and melilite, the latter being a solid solution of gehlenite phase (C_2AS) and akermanite phase (C_2MS_2). In this study, the oxides contained in these crystalline phases are subtracted from the total oxides because they are not hydraulic, so that only the oxides in glass form are considered to react. These oxides are assumed to be the only reactive part of the slag, which will hydrate congruently, and the crystalline phases are considered to be inert during the hydration of slag.

Three reaction models for quantifying the hydration products and determining the composition of the main hydration product (C–S–H) are proposed based on the molar balances of the oxides between the starting material (in glass) and the hydration products. These models consider different degrees of aluminum substitution for silicon in C–S–H. For simplification purpose two assumptions are introduced into the models:

1. A slag grain is a homogeneous mixture of all oxides; only the oxides in the glass are reactive (i.e., oxides in the crystal part are inert).
2. All oxides in the glass react congruently to a number of hydration products which are selected based on the observations in experiments in literature.

Among the selected hydration products (C–S–H, M_5AH_{13}, $C_6AFS_2H_8$, $C_6A\bar{S}_3H_{32}$, C_4AH_{13} and C_2ASH_8), hydrotalcite is the only magnesium-containing phase and all M reacts into it. Similarly, all iron oxide reacts into the hydrogarnet phase and all sulfates into ettringite.

Based on the chemical formula of each hydration product (Table 1), mole balances of major oxides in the product are readily determined. Water contents of the hydration products in different hydration states are also included in Table 1 based on the discussions in previous sections.

Using the molar balance of each oxide between the starting material and the hydration products, Eqs. (2)–(7) are established:

$$a \cdot n_{C-S-H} + 6n_{HG} + 6n_{AFt} + 4n_{AH} + 2n_{ST} = y_C \quad (2)$$

$$n_{C-S-H} + 2n_{GH} + n_{ST} = y_S \quad (3)$$

$$b \cdot n_{C-S-H} + n_{HT} + n_{HG} + n_{AFt} + n_{AH} + n_{ST} = y_A \quad (4)$$

$$3n_{AFt} = y_{\bar{S}} \quad (5)$$

$$5n_{HT} = y_M \quad (6)$$

$$n_{HG} = y_F \quad (7)$$

in which $n_{C\text{-}S\text{-}H}$, n_{HT}, n_{HG}, n_{AFt}, n_{AH} and n_{ST} are the moles (per gram slag) of the hydration products C–S–H, hydrotalcite, hydrogarnet, ettringite, tetracalcium aluminate hydrate and strätlingite, respectively; y_C, y_S, y_A, y_M, $y_{\bar{S}}$, and y_F are moles of the oxides

Table 1 Molar balance of oxides in hydration products

Hydration product	Mole	Molar balance								
		C	S	A	M	$\bar{S}$	F	H (105 °C)	H (80% RH)	H (100% RH)
$C_aA_bH_x$	$n_{C\text{-}S\text{-}H}$	a	1	b				1.2	a + 0.8	a + 1.5
M_5AH_{13}	n_{HT}			1	5			7[a]	13[a]	19[a]
$C_6AFS_2H_8$	n_{HG}	6	2	1			1	8	8	18
$C_6A\bar{S}_3H_{32}$	n_{AFt}	6		1		3		8	32	32
C_4AH_{13}	n_{AH}	4		1				7	13	19
C_2ASH_8	n_{ST}	2	1	1				8	8	8

[a] Estimated value assuming the hydrotalcite and the tetracalcium aluminate hydrate have the same dehydration characteristics, see text

contained in the glass content of the slag (per gram of slag), which are calculated from the masses of oxides in the glass and their molar masses. From Eqs. (5) to (7) quantities of the hydrotalcite phase, ettringite and the hydrogarnet phase readily follow that:

$$n_{AFt} = y_{\bar{S}}/3 \tag{8}$$

$$n_{HT} = y_M/5 \tag{9}$$

$$n_{HG} = y_F \tag{10}$$

Substituting n_{AFt}, n_{HT} and n_{HG} from Eqs. (8)–(10) into Eqs. (2)–(4) yields:

$$a \cdot n_{C-S-H} + 4n_{AH} + 2n_{ST} = y_C - 2y_{\bar{S}} - 6y_F = y_C^* \tag{11}$$

$$n_{C-S-H} + n_{ST} = y_S - 2y_F = y_S^* \tag{12}$$

$$b \cdot n_{C-S-H} + n_{AH} + n_{ST} = y_A - y_{\bar{S}}/3 - y_M/5 - y_F = y_A^* \tag{13}$$

in which y_C^*, y_S^* and y_A^* practically represent the quantities of C, S and A available for the hydration products C–S–H and the AFm phases (C_4AH_{13} and C_2ASH_8). By eliminating $n_{C\text{-}S\text{-}H}$ from Eqs. (11) to (13), the following equations are obtained:

$$4n_{AH} + (2 - a) \cdot n_{ST} = y_C^* - a \cdot y_S^* \tag{14}$$

$$n_{AH} + (1 - b) \cdot n_{ST} = y_A^* - b \cdot y_S^* \tag{15}$$

Solving Eqs. (14) and (15) simultaneously gives:

$$n_{AH} = \frac{(1-b)y_C^* - (a-2b)y_S^* - (2-a)y_A^*}{a - 4b + 2} \tag{16}$$

$$n_{ST} = \frac{-y_C^* + (a-4b)y_S^* + 4y_A^*}{a - 4b + 2} \tag{17}$$

Substituting n_{AH} and n_{ST} from Eqs. (16) and (17) into Eq. (11), $n_{C\text{-}S\text{-}H}$ now reads:

$$n_{C-S-H} = \frac{y_C^* + 2y_S^* - 4y_A^*}{a - 4b + 2} \tag{18}$$

In the system above (Eqs. (16)–(18)), there are five unknowns and three equations. Therefore, extra conditions are needed to solve the system. As the C_4AH_{13} and C_2ASH_8 are rarely found simultaneously in the mature AAS pastes in experiments, their formations are considered alternatively, corresponding to different cases in the models. Furthermore, various degrees of A substitution in C–S–H are considered.

First, a model, namely Model 1, is proposed, in which no aluminum substitution for silicon in C–S–H is considered. This model is a simplified one for that the A substitution for S most likely takes place in AAS pastes. Then, the aluminum substitution in C–S–H is accounted for. The molar balances of C, S and A in C–S–H are prescribed by the relation proposed by Richardson [11] (Eq. (1)). Accordingly, another model, namely Model 2, is proposed. For some slags no AFm phases are formed in their hydration products. Hence, the third model, namely Model 3, is proposed. The C/S and A/S ratios in the hydration product C–S–H are taken to be free in this model. In all three models proposed, the quantities of the hydrotalcite phase, ettringite and the hydrogarnet phase always follow from Eqs. (8), (9) and (10), respectively.

Model 1: no aluminum substitution for silicon in C–S–H

In this simplified model, no A substitution for S in C–S–H is considered. Hence, $b = 0$ in Eqs. (11)–(13). The quantities of C_4AH_{13}, C_2ASH_8 and C–S–H are now calculated from Eqs. (16)–(18) as:

$$n_{AH} = \frac{y_C^* - a y_S^* - (2-a) y_A^*}{a+2} \quad (19)$$

$$n_{ST} = \frac{-y_C^* + a y_S^* + 4 y_A^*}{a+2} \quad (20)$$

$$n_{C-S-H} = \frac{y_C^* + 2 y_S^* - 4 y_A^*}{a+2} \quad (21)$$

Now the system contains three equations (Eqs. (19)–(20)) and four unknowns (n_{AH}, n_{ST}, $n_{C\text{-}S\text{-}H}$ and a). In the following discussion, two cases are distinguished, depending on the formation of either C_4AH_{13} or C_2ASH_8.

First, the case considering the formation of C_4AH_{13} is investigated, namely Case 1. Since no strätlingite is formed, $n_{ST} = 0$. From Eq. (20), it follows that:

$$-y_C^* + a \cdot y_S^* + 4 y_A^* = 0 \quad (22)$$

Now, the C/S ratio (a) reads:

$$a = \frac{y_C^* - 4 y_A^*}{y_S^*} \quad (23)$$

Using the C/S ratio calculated from Eq. (23), $n_{C\text{-}S\text{-}H}$ and n_{AH} are calculated as:

$$n_{AH} = y_A^* \quad (24)$$

$$n_{C-S-H} = y_S^* \quad (25)$$

Equations (24) and (25) show that the quantities of C_4AH_{13} and C–S–H are readily determined by the available A and S contents from the slags.

Then, as the second case, namely Case 2, the formation of C_2ASH_8 is considered and C_4AH_{13} is excluded from the hydration products, indicating $n_{AH} = 0$. Based on Eq. (19), the following equation is yielded:

$$y_C^* - a \cdot y_S^* - (2-a) y_A^* = 0 \quad (26)$$

Now, the C/S ratio (a) reads:

$$a = \frac{y_C^* - 2 y_A^*}{y_S^* - y_A^*} \quad (27)$$

Similarly, substituting a into Eqs. (20) and (21) gives n_{ST} and $n_{C\text{-}S\text{-}H}$ as:

$$n_{C-S-H} = y_S^* - y_A^* \quad (28)$$

$$n_{ST} = y_A^*. \quad (29)$$

In this model, for both cases the quantity of the AFm phase (C_4AH_{13} or C_2ASH_8) equals the amount of the available A from the slags. No aluminum substitution for silicon is considered to take place in C–S–H. As a consequence, there is more A available for the formation of the AFm phases, which consumes C. Therefore, there is less C available for the formation of C–S–H and the predicted C/S ratio will be lower than the measured values in C–S–H.

Model 2: the C/S and A/S ratios in C–S–H are coupled by the relation proposed by Richardson

As observed in experiments on the reaction of AAS, A enters the hydration product C–S–H and substitutes for S in the bridging tetrahedra of the dreierkette chains. So incorporating the A substitution for S in C–S–H is important for modelling the reaction of AAS. In this model, the C/S ratio (a) and A/S ratio (b) in the C–S–H are coupled by the relation proposed by Richardson (Eq. (1)). The relation is further written as:

$$b = (1 - 0.4277a)/4.732 \quad (30)$$

Similarly, two cases are considered, corresponding to the formation of C_4AH_{13} or C_2ASH_8, respectively. First, Case 1, the case considering the formation of C_4AH_{13}, is considered, indicating $n_{ST} = 0$. Thus, from Eq. (20) the following equation is obtained:

$$-y_C^* + (a - 4b) y_S^* + 4 y_A^* = 0 \quad (31)$$

By solving Eqs. (30) and (31) simultaneously, the C/S ratio is calculated as:

$$a = \frac{y_C^* + 0.85 y_S^* - 4 y_A^*}{1.36 y_S^*} \quad (32)$$

and the A/S ratio is calculated from Eq. (30) as:

$$b = \frac{-0.43 y_C^* + 0.99 y_S^* + 1.72 y_A^*}{7.54 y_S^*}. \quad (33)$$

In this case, the quantity of C–S–H follows from Eq. (12) with $n_{ST} = 0$. n_{AH} is solved from Eq. (15) as:

$$n_{AH} = y_A^* - b \cdot y_S^* \quad (34)$$

Because $n_{AH} \geq 0$ is valid for all slags, the following inequality is yielded:

$$b \leq y_A^*/y_S^* \quad (35)$$

Substituting Eq. (33) into inequality (35) gives the condition for the formation of C_4AH_{13} as:

$$5.82y_A + 0.43y_C \geq 0.99y_S + 1.164y_M + 6.42y_F + 2.8y_{\bar{S}} \quad (36)$$

Converting inequality (36) into the mass fraction of oxides in the slag yields:

$$x_A + 0.13x_C \geq 0.29x_S + 0.51x_M + 0.70x_F + 0.61x_{\bar{S}} \quad (37)$$

Increasing the mass fractions of oxides on the left side has a positive influence on the formation of C_4AH_{13}; for the right side negative influence is expected. Hence, conclusion can be drawn from inequality (37): The AFm phase is most likely formed in the hydration products from slags rich in C and A, or poor in S, M, F or $\bar{S}$.

Case 2 considers the formation of C_2ASH_8 and excludes C_4AH_{13} from the hydration products, indicating $n_{AH} = 0$. Again from Eq. (19) it follows:

$$(1-b)y_C^* - (a-2b)y_S^* - (2-a)y_A^* = 0 \quad (38)$$

Together with Eq. (30), the C/S ratio (a) can be solved as:

$$a = \frac{y_C^* + 0.53y_S^* - 2.53y_A^*}{-0.11y_C^* + 1.5y_S^* - 1.27y_A^*}. \quad (39)$$

Again, the A/S ratio (b) can be calculated from Eqs. (30) and (39) as:

$$b = 0.21 + \frac{0.09(y_C^* + 0.53y_S^* - 2.53y_A^*)}{-0.11y_C^* + 1.5y_S^* - 1.27y_A^*}. \quad (40)$$

The quantity of C_2ASH_8 is calculated from Eq. (17) as:

$$n_{ST} = (y_A^* - by_S^*)/(1-b) \quad (41)$$

The quantity of C–S–H follows from Eq. (18). Similar to Case 1, since strätlingite is formed, $n_{ST} \geq 0$. Substituting Eq. (41) into the inequality yields the same inequality as (35).

Inequality (35) indicates that the aluminum substitution degree in C–S–H is limited to a certain degree. This degree depends on the mineral composition of the slag, or more precisely, by the available A and S from the slag to form C–S–H and the AFm phases. This conclusion on the limit of the aluminum substitution degree in C–S–H is in line with the observation of Wang and Scrivener [10]. They found silicon ions are occupying some of the bridging tetrahedral of the dreierkette structure in C–S–H. The aluminum substitution degree was limited due to the amount of aluminum available instead of any intrinsic limit. The authors concluded that the aluminum content from slags was firstly combined with magnesium in the hydrotalcite or potentially with calcium in the AFm phase rather than entering the C–S–H phase and increasing its A/C ratio.

Therefore, the aluminum substitution degree as coupled by Eq. (1) is the highest state of substitution. Equation (1) should be used if the slag is relatively rich in C and A, or poor in the other oxides. If the maximum substitution degree is obtained, the remaining A combines with C (and S in the case of C_2ASH_8) to form the AFm phase. The actual substitution degree is thus determined by the amount of aluminum available. If the degree of aluminum substitution is overestimated (for example, in Eq. (1)) and exceeds the limit as prescribed by inequality (35), a negative value for the quantity of the AFm phase is yielded in this model.

Model 3: no AFm phases are formed and the substitution degree is free

Preliminary calculations using Model 2 show that, for some slags the quantity of AFm phases (C_4AH_{13} or C_2ASH_8) may result in negative values, indicating the failure of Model 2 for these slags. The courses for these negative values are discussed in previous sections. In such cases, an alternative model is put forward, namely Model 3. As observed in some hardened AAS pastes, C_4AH_{13} nor C_2ASH_8 were found, indicating that neither of them was formed. Therefore, Model 3 is proposed, in which the aluminum substitution for silicon in C–S–H is taken into account and no AFm phases are formed. The C/S and A/S ratios in C–S–H are no longer coupled by Eq. (1) and are taken to be free. Because no AFm phases are formed, $n_{AH} = 0$ and $n_{ST} = 0$. Now solving Eqs. (31) and (38) simultaneously gives the C/S ratio (a) and A/S ratio (b) in C–S–H as:

$$a = y_C^*/y_S^* \quad (42)$$

$$b = y_A^*/y_S^* \quad (43)$$

and the quantity of C–S–H follows from Eq. (18). The results derived from Model 3 are positive for all slags. On the other hand, with some slags the A substitution degree (A/S) might exceed the maximum degree as by Eq. (30). In such cases, Model 2 is used.

As a whole, Model 2 is always recommended to model the hydration of slags under investigation. If it is not applicable, most likely for slags poor in C and A, or rich in S, M, F or $\bar{S}$, Model 3 is used. The choice of models can be made beforehand using Eq. (36).

Experimental validation of the models

To evaluate the proposed models, three slags are taken from literature, which were tested employing different techniques. The oxide compositions of these slags are listed in Table 2. The oxides in the selected hydration products, i.e., S, C, A, M, $\bar{S}$ and F, are normalized to a total percentage of 100% (Table 3). The molar mass of each slag is also included, which is defined as:

$$M_{sl} = \frac{\Sigma y_i \cdot M_i}{\Sigma y_i} \tag{44}$$

in which i stands for the oxides C, S, A, M, etc. It can be seen that the molar mass of each slag takes the value between M_C and M_S since C and S are the most abundant oxides in the glass content of slags (see Table 3). The C/S and A/S ratios (in moles) in the glass content of the unhydrated slags are included in Table 3 as well. No crystalline phases in significant amounts were detected in all three slags, so that all oxides are in the glass form and reactive.

Slag 1 was taken from the work of Richardson and Groves [14], in which techniques of transmission electron microscopy (TEM) combined with electron microprobe analysis (EMPA) were used to analyze hydration products of slag blended cement with different slag proportions. C–S–H was found to be the most dominant product in both the ''inner product'' and the ''outer product''. The inner product of slag grains contained C–S–H of the same composition as the outer product C–S–H. It is closely mixed with an M–A rich hydrotalcite phase. In the pure slag system (water activated), the C/S ratio in C–S–H was 1.18 and the A/S ratio was 0.11. No AFm phases were found in the pure GGBFS system although they were detected in the blended cement pastes.

Table 2 Oxide compositions of the three slags

Oxide	Slag 1 (mass %)	Slag 2 (mass %)	Slag 3 (mass %)
C	41.7	40.2	41.45
S	37.2	35.5	35.5
A	11.0	12.6	12.15
M	7.74	9.0	8.34
$\bar{S}$	3.68	0	0.18
F	0.38	0.6	1.01
N	0.64	0	0.58
K	0.55	0	0.64
Total	102.89	97.9	99.85

The slags are taken from Richardson and Groves [14], Wang and Scrivener [5] and Brough and Atkinson [7]. All oxides are in the glass form because no crystalline phases in significant amount are detected

Table 3 Oxide compositions in the glass content of the three slags from Table 2 together with their molar fractions and molar mass

Oxide	Slag 1		Slag 2		Slag 3		M
	mass %	mole %	mass %	mole %	mass %	mole %	
C	41.0	43.5	41.2	43.3	42.0	44.4	56.1
S	36.6	36.2	36.2	35.6	36.0	35.5	60.1
A	10.8	6.3	12.9	7.4	12.3	7.2	102.0
M	7.6	11.2	9.2	13.5	8.5	12.4	40.3
$\bar{S}$	3.6	2.7	0	0	0.2	0.1	80.1
F	0.4	0.1	0.5	0.2	1.0	0.4	159.6
Total	100	100	100	100	100	100	–
C/S	1.12	1.20	1.14	1.22	1.17	1.25	–
A/S	0.26	0.15	0.31	0.17	0.29	0.16	–
M_{sl}	59.46		59.01		59.27		–

Minor compositions are omitted; only oxides present in selected hydration products, namely C, S, A, M, $\bar{S}$ and F, are listed. The mass fractions are normalized to a total of 100%. The molar mass of slag (M_{sl}) is calculated using Eq. (44)

Slag 2 was taken from the work of Wang and Scrivener [5]. SEM/BSE combined with EDX microanalysis together with XRD was used in this research. C–S–H is the main hydration product regardless of the activator used. Hydrotalcite was formed as well in the AAS paste. C_4AH_{13} was observed while no C_2ASH_8 was found. The A/C ratio in the C–S–H was 0.08 at 1 day and increased slightly to 0.10 at 1 year.

Slag 3 was taken from the work of Brough and Atkinson [7]. Hydration products of slags activated with water glass and potassium hydroxide (KOH) solution were analyzed by using SEM equipped with EDX and ^{29}Si magic angle spinning nuclear magnetic resonance (MAS NMR) together with XRD. The NMR results showed long-chain substituted C–S–H. The C/S ratio in C–S–H was highly variable if activated with water glass, and was about 1.1 if activated with the KOH solution. Here, only the data obtained in hardened paste activated with the KOH solution are used because silicon is introduced into the system when the water glass is used as activator. The A/S ratio measured in the KOH-activated slag was 0.125 at 1 year. Hydrotalcite was formed in the inner product with an M/A ratio of 5.6. C_4AH_{13} or a similar phase was found in small quantities in the KOH-activated paste.

In the works above, the oxide compositions of the slags are all given in mass fractions. They are firstly converted into molar contents as $y_i = x_i/M_i$, in which i is

the oxide in the slag (C, S, A, etc., respectively); y_i and x_i is the mole content (mole/g) and mass fraction of oxide i in the slag, respectively; M_i is the molar mass of oxide i.

First, Model 1 is applied to all three slags. Quantities of the hydration products (in mole percentages) and the C/S ratio in C–S–H calculated using Model 1 are listed in Table 4. Apparently, C–S–H is the most abundant product. Hydrotalcite exists in a significant amount as well. For all three slags, the C/S ratios corresponding to the formation of C_2ASH_8 (Case 2) accord well with the observations in hardened AAS pastes, whereas C/S ratios corresponding to the formation of C_4AH_{13} (Case 1) are generally lower than the measurements. The difference comes from the different calcium content in the two products: C_4AH_{13} contains comparably more C than C_2ASH_8, so less C is available for C–S–H.

Then, Model 2 is applied to the three slags. Quantities of the hydration products (in mole percentage) and the C/S and A/S ratios in C–S–H calculated using Model 2 are listed in Table 5. The C/S and A/S ratios calculated using Model 2 with all three slags agree relatively better with the measurements if compared to the results using Model 1. However, the quantity of the AFm phase for Slag 1 results in a negative value. The negative value indicates that this phase is unlikely formed in the mature paste, which is consistent with the experimental observation.

Comparing the oxide compositions of the three slags, one can see that Slag 2 and Slag 3 are relatively rich in A as compared with Slag 1. Thus, as discussed previously, the AFm phases can only be formed when there is enough A from the slag to achieve the maximum substitution degree for silicon in C–S–H. It is more likely formed from slags rich in A. Because A is also combined with M to form hydrotalcite, the hydration of slags poor in M probably also forms the AFm phase.

Table 4 Quantities of hydration products and C/S ratio in C–S–H calculated using Model 1

Hydration product	Slag 1 (mole %)		Slag 2 (mole %)		Slag 3 (mole %)	
	Case 1	Case 2	Case 1	Case 2	Case 1	Case 2
$C_aSA_bH_x$	85.06	83.91	82.55	80.46	82.91	80.98
M_5AH_{13}	5.32	5.73	6.31	7.06	5.94	6.61
$C_6AFS_2H_8$	0.33	0.36	0.44	0.50	0.91	1.01
$C_6A\bar{S}_3H_{32}$	2.12	2.28	0	0	0.11	0.12
C_4AH_{13}	7.17	0	10.70	0	10.13	0
C_2ASH_8	0	7.72	0	11.98	0	11.28
Total	100	100	100	100	100	100
C/S (*a*)	0.70	0.95	0.68	1.08	0.72	1.09
C/S Mea.	1.18		1.2		1.1	
A/S Mea.	0.112		0.12		0.125	

In Case 1 only the formation of C_4AH_{13} is considered and in Case 2 the formation of C_2ASH_8. The measured C/S ratios by Richardson and Groves [14], Wang and Scrivener [5] and Brough and Atkinson [7] in C–S–H are also included

Table 5 Quantities of hydration products, C/S and A/S ratios in C–S–H calculated using Model 2

Hydration product	Slag 1 (mole %)		Slag 2 (mole %)		Slag 3 (mole %)	
	Case 1	Case 2	Case 1	Case 2	Case 1	Case 2
$C_aSA_bH_x$	89.6	89.2	90.8	89.9	91.1	90.4
M_5AH_{13}	5.6	5.4	6.9	7.1	6.5	6.6
$C_6AFS_2H_8$	0.3	0.3	0.5	0.5	1.0	1.0
$C_6A\bar{S}_3H_{32}$	2.2	2.1	0	0	0.1	0.1
C_4AH_{13}	–2.2	0	1.8	0	1.3	0
C_2ASH_8	0	–3.0	0	2.5	0	1.9
Total	95.5	94.0	100	100	100	100
C/S (*a*)	1.14	1.07	1.12	1.17	1.15	1.19
A/S (*b*)	0.109	0.115	0.110	0.105	0.108	0.104
C/S Mea.	1.18		1.2		1.1	
A/S Mea.	0.112		0.12		0.125	

In Case 1 only the formation of C_4AH_{13} is considered and in Case 2 the formation of C_2ASH_8. The measured C/S ratios by Richardson and Groves [14], Wang and Scrivener [5] and Brough and Atkinson [7] in C–S–H are also included

To determine the formation of C_2ASH_8 or C_4AH_{13} theoretically in the mature AAS pastes is difficult. Thermodynamically C_2ASH_8 is stable with respect to C_4AH_{13} [28]. But the existence of C_4AH_{13} is more commonly found in mature AAS pastes. The reason for the formation of C_4AH_{13} rather than C_2ASH_8 in mature AAS pastes is unclear. The high alkalinity of pore solution in the AAS paste probably favours the formation of C_4AH_{13}. Also anion exchange may take place and actually a solid solution of the AFm phases is formed. The AFm phases are generally closely mixed with C–S–H and are hard to characterize.

As a whole, Model 2 gives satisfactory results if compared to Model 1. The AFm phase (C_4AH_{13} or C_2ASH_8) is assumed in this model to be formed, which is not valid for slags low in A or high in M. For the slags that Model 2 is not valid, Model 3 should be used for modelling.

Similarly, Model 3 is applied to the three slags selected. Neither C_4AH_{13} nor C_2ASH_8 is formed in the hydration products in this model. The C/S and A/C ratios in C–S–H are taken to be free. Quantities of the hydration products (in mole percentages) and the C/S and A/S ratios in C–S–H calculated using Model 3 are listed in Table 6. For all three slags, the predicted C/S and A/S ratios in C–S–H are consistent with the

Table 6 Quantities of hydration products, C/S and A/S ratios in C–S–H calculated using Model 3

Hydration product	Slag 1 (mole %)	Slag 2 (mole %)	Slag 3 (mole %)
$C_aSA_bH_x$	91.63	92.44	92.26
M_5AH_{13}	5.73	7.06	6.61
$C_6AFS_2H_8$	0.36	0.50	1.01
$C_6A\bar{S}_3H_{32}$	2.28	0	0.12
C_4AH_{13}	0	0	0
C_2ASH_8	0	0	0
Total	100	100	100
C/S (*a*)	1.04	1.20	1.20
A/S (*b*)	0.084	0.130	0.122
C/S Mea.	1.18	1.2	1.1
A/S Mea.	0.112	0.12	0.125

No AFm phases are formed in this model. The measured C/S ratios by Richardson and Groves [14], Wang and Scrivener [5] and Brough and Atkinson [7] in C–S–H are also included

experimental observations. They vary slightly from the predictions of Model 2. The A/S ratios calculated with Slag 2 and 3 are slightly higher than the predictions of Model 2. Since in Model 2 the AFm phases are formed, containing some A in it, less A is available for the C–S–H and the A/S ratio will be lower. As a whole, the C/S and A/S ratios calculated using Model 3 accord well with the experimental observations. Model 3 can be used if Model 2 is not valid for quantifying hydration products and determining the composition of C–S–H.

A schematic comparison between the measured and predicted C/S and A/S ratios in the hydration product C–S–H are shown in Fig. 1a (C/S ratio) and 1b (A/S ratio). The C/S and A/S ratios (in moles) in the unhydrated slag are included in the figures as well. Values of C/S and A/S ratios as results of Model 1 and Model 2 are taken from the average values from Case 1 and Case 2. On the one hand, the C/S and A/S ratios in C–S–H predicted using the proposed models are generally in good agreement with the experimental observations. For Model 1, slightly lower values are predicted. On the other hand, these values differ considerably from the molar ratios of the respective oxides in the starting material. Therefore, for predicting the composition of C–S–H, the C/S and A/S ratios in the slags can not be used directly, although C–S–H is obviously the most dominant product of slag hydration. The presence of the other hydration products, i.e., hydrotalcite, ettringite, hydrogarnet and AFm phases (if formed) obviously influences the composition of the main hydration product C–S–H, even though, as a total, they amount to approximately 10% in moles. This influence is more prominent on the A/S ratio in C–S–H.

Since A is contained in all hydration products considered, its distribution can be used as a indicator for

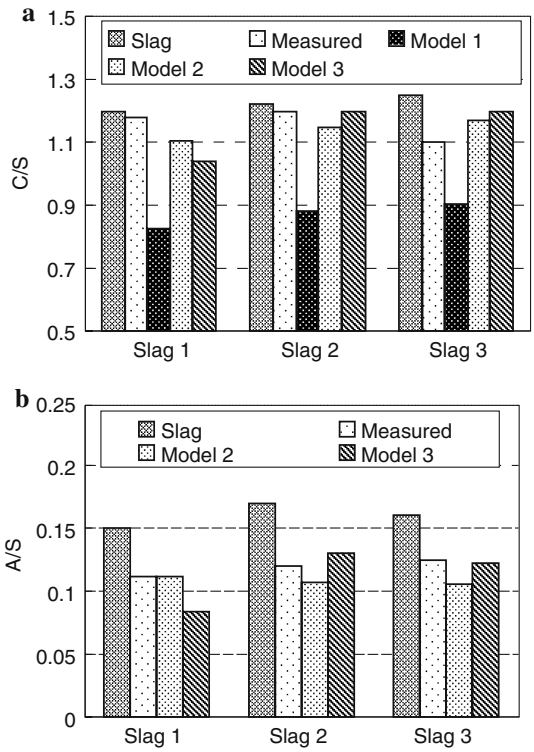

Fig. 1 (**a**) The C/S ratio in the slag and in the hydration product C–S–H: measured and predicted. The measurements are taken from the experimental data by Richardson and Groves [14], Wang and Scrivener [5] and Brough and Atkinson [7]. (**b**) The A/S ratio in the slag and in the hydration product C–S–H: measured and predicted. The measurements are taken from the experimental data by Richardson and Groves [14], Wang and Scrivener [5] and Brough and Atkinson [7]

the relative amounts of the hydration products. The distribution of A from slags in the hydration products is analyzed and is shown in Fig. 2. For Slag 1 the results from Model 3 and for Slag 2 and 3 the results from Model 2, Case 1 are used. The option of Case 1 or 2 in Model 2 does not make much difference because in both cases the AFm phase amounts less than 3% in moles and actually differs less than 1% from each other. A large part of A from the slag is shown in Fig. 2

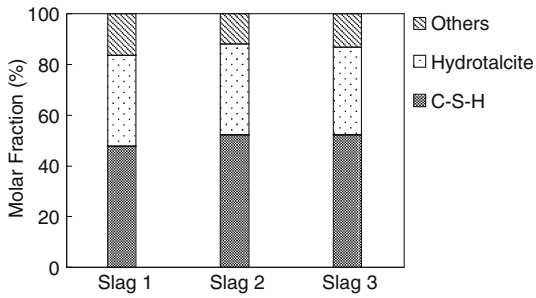

Fig. 2 The fraction of A from the slag that enters the C–S–H, hydrotalcite and all other products

to enter the main hydration product C–S–H. Its quantity is comparable with that entering the other hydration products. Thus, the consideration of A substitution for S in C–S–H is of essential importance when modelling the hydration of AAS. The amount of A contained in the hydrotalcite is also remarkable, because of its relatively large amount (see Table 4–6). Research has shown that the amount of aluminum in the slags might have a dominant influence on the reactivity of slags [29]. An obvious relationship was observed between its distribution in the hydration products and the mechanical properties of slag cement mortars [30]. Using the models proposed in this study, the role of A from the slag in the hydration products can be clarified, providing opportunities for further revealing the influence of the oxide compositions on the reactivity of a slags.

Water retention

When the quantities of all hydration products are calculated using the proposed model, the retained water in these products are concomitantly obtained, rendering the possibility of deriving the occurring reactions of AAS. The amount of retained water in the hydration products is calculated as:

$$n_{\mathrm{H}} = \sum(\mathrm{H}_i \cdot n_i) \tag{45}$$

in which n_{H} is the retained water in the hydration product (mole per gram slag); H_i is the water content in the hydration product, which is dependent on the hydration states and can be taken from Table 1; n_i is the quantity of the hydration product calculated using the proposed models.

The hydration reaction of AAS is thus written as:

$$\begin{aligned}\mathrm{C}_{y_{\mathrm{C}}}\mathrm{S}_{y_{\mathrm{S}}}\mathrm{A}_{y_{\mathrm{A}}}\mathrm{M}_{y_{\mathrm{M}}}\bar{\mathrm{S}}_{y_{\bar{\mathrm{S}}}}\mathrm{F}_{y_{\mathrm{F}}} + n_{\mathrm{H}}\mathrm{H} \rightarrow\ & n_{\mathrm{C-S-H}}\mathrm{C}_a\mathrm{SA}_b\mathrm{H}_x \\ & + n_{\mathrm{HT}}\mathrm{M}_5\mathrm{AH}_{13} + n_{\mathrm{HG}}\mathrm{C}_6\mathrm{AFS}_2\mathrm{H}_8 + n_{\mathrm{AFt}}\mathrm{C}_6\mathrm{A}\bar{\mathrm{S}}_3\mathrm{H}_{32} \\ & + n_{\mathrm{AH}}\mathrm{C}_4\mathrm{AH}_{13} + n_{\mathrm{ST}}\mathrm{C}_2\mathrm{ASH}_8.\end{aligned} \tag{46}$$

Note that in the hydration equation above general formula of hydration products are used, although their water content might vary in different hydration states. The retained water in the hydration products in respective hydration states for the selected three slags is listed in Table 7. Again, for Slag 1 the results from Model 3 and for Slag 2 and 3 the results from Model 2, Case 1 are used. The retained water in the hydration products of AAS in the saturated state is prominently higher than that of typical OPC, about 0.44 g/g cement reacted at 100% RH [12]. This higher water content is consistent with the larger mass percentage of water in the hydration products hydrotalcite (about 53%) considering its relatively large amount. Collins and Sanjayan [31] also observed this higher water retention capability of AAS paste than OPC. Therefore, for achieving high degree of AAS hydration, probably larger initial water/binder (w/b) ratio than that of Portland cement can be preferential.

Table 7 Retained water in the hydration products in different hydration states (g/g slag reacted)

Hydration state	Slag 1	Slag 2	Slag 3
105 °C	0.21	0.20	0.20
80% RH	0.39	0.33	0.33
100% RH	0.51	0.47	0.47

The non-evaporable water of fully hydrated slags is around 0.20 g/g slag reacted. This value is in good agreement with the measurement by Song and Jennings [32], i.e., 19.3% referred to the ignited mass, and also with the measurement by Wolhuter et al. [33], i.e., 0.19 g/g slag reacted. In contrast to the saturated situation, the non-evaporable water of AAS (after being dried at 105 °C) is apparently lower than that of OPC, about 0.23 g/g cement reacted [12].

The procedure for deriving the hydration equation of the slag is summarized as:

1. Calculating or measuring the oxide composition in the glass part of slag;
2. Calculating the quantities of ettringite, hydrotalcite and hydrogarnet using Eqs. (8)–(10).
3. Calculating the remaining C, S and A available for the other hydration products using Eqs. (11)–(13).
4. Substituting the available quantity of C, S and A into Model 1, 2 or 3 in corresponding cases, yielding the C/S ratio (and A/S ratio in Model 2 and 3) in C–S–H and the quantities of $\mathrm{C_4AH_{13}}$ (or $\mathrm{C_2ASH_8}$) and C–S–H.
5. Calculating the water retention by the hydration products of slag in respective hydration states using Eq. (45).
6. Writing the hydration equation of slag using Eq. (46).

Chemical shrinkage

Chemical shrinkage is the volume reduction of the paste as the consequence of the chemical reaction of the reactant and water. Generally, the total volume of the reaction product is smaller than that of the starting

materials, exhibiting an inherent shrinkage. Together with other hydration characteristics of the hardening cementitious system such as the non-evaporable water and heat evolution, chemical shrinkage is commonly used to evaluate its hydration degree. After the quantities of major hydration products are determined using the proposed models, their total volume can be obtained, enabling the calculation for the chemical shrinkage of AAS. Physical properties of the hydration products are listed in Table 8. At present some properties of the hydration products are not available. In this study, they are extrapolated assuming the gel water (water in the products and other than the non-evaporable water) has a molar volume of 16.2 cm^3/mol, which has been proven to provide reasonable agreement with available data [18–20, 25]. The physical properties of C–S–H are even more complex than the others. In this study, the release/adsorption of water by C–S–H in different hydration states is assumed not to change its molar volume. The density of C–S–H in the saturated state is calculated as a function of the C/S ratio of C–S–H as [18, 19, 25]:

$$\rho_{C-S-H} = \frac{87.12 + 74.10a}{38.42 + 33.05a}. \quad (47)$$

Note in Eq. (47) the A/S ratio is not included because at present the influence of A on the physical properties of C–S–H is not clear. Here, incorporating A into the C–S–H is assumed not to significantly change its density. Since incorporating A into the C–S–H will increase its molar mass, the molar volume of C–S–H is influenced. In severer hydration states, for example, oven drying at 105 °C or 80% RH, the C–S–H is dehydrated. Release of water from C–S–H in different hydration states can hardly change its volume [18, 19, 25]. Thus, in different hydration states, the molar volume of C–S–H most likely stays constant.

The chemical shrinkage is defined as the volume reduction per mass of reacted slag as:

$$\Psi_S = \frac{(V_{sl} + V_H) - V_{hp}}{m_{sl}} = \frac{(m_{sl}/\rho_{sl} + n_H \cdot \omega_H) - \sum n_i \omega_i}{m_{sl}} \quad (48)$$

in which i stands for the hydration products; ω is the molar volume of the substances. The amount of water in the products is taken from Table 7. Moles of hydration products are taken from Table 6 (Slag 1) and Table 5 (Slag 2 and 3) considering different hydration states. The density of the slag is taken to be 2.92 g/cm^3. The chemical shrinkages of the three selected slags are calculated using Eq. (48) (Table 9).

As can be seen from the model predictions, the hydration of AAS has much larger chemical shrinkage than OPC in the saturated state (approximately 6–9.9 ml/100 g binder according to Powers and Brownyard [34], Köster and Odler [35], Mills [36], Czernin [37], Tazawa et al. [38]). It is also larger in other hydration states although actually the chemical shrinkage of cement paste in these states can hardly be measured. Larger shrinkage of AAS paste/mortar than OPC was observed in various studies [31, 39]. Since the chemical shrinkage normally increases the pore volume in the paste with hardly any external volume change, the shrinkage might have a dominant influence in the micro scale. As a result of the self-restraint (when aggregate is present), internal stress might develop due to the chemical shrinkage. Microcracks in the structure can take place, which is observed in various experiments [39, 40].

Microstructure and porosity

Amongst other microstructural characteristics of AAS paste, such as composition, distribution and amount of

Table 8 Physical properties of hydration products

Substance	M (g/mole)			ρ (g/cm^3)			ω (cm^3 /mole)		
	105 °C	80% RH	100% RH	105 °C	80% RH	100% RH	105 °C	80% RH	100% RH
C–S–H	Var.	Var.	Var.	Var.	Var.	Var.	Var.	Var.	Var.
M_5AH_{13}	429.5	537.5	645.50	2.62	2.06[b]	1.80	163.72[c]	260.92	358.12[c]
$C_6AFS_2H_8$	862.4	862.4	1042.4	3.03	3.03[a]	2.24[a]	284.62	284.62	465.36
$C_6A\bar{S}_3H_{32}$	822.9	1254.9	1254.9	2.38	1.78[a]	1.78	345.76[c]	705.0	705.0
C_4AH_{13}	452.4	560.4	668.40	2.53[a]	2.05[a]	1.80[a]	176.17	273.37	371.33
C_2ASH_8	418.3	418.3	418.30	1.94[a]	1.94	1.94	215.62	215.62	215.62
H	18.0			1.0			18.0		

[a] Brouwers [19, 25]

[b] Taylor [12]

[c] Based on that molar volume of the gel water is 16.22 cm^3/mole

Table 9 Chemical shrinkage of AAS in different hydration states (ml/100 g slag reacted)

Hydration state	Slag 1	Slag 2	Slag 3
105 °C	– 5.9	– 2.0	– 2.0
80% RH	3.3	5.9	5.8
100% RH	11.5	13.9	13.7

hydration product, the presence of another phase in the paste, pore, is of essential importance while evaluating the performance of AAS. The porosity, pore size distribution and connectivity of pores can strongly influence the mechanical properties of the paste. With the quantities of the hydration products and the composition of C–S–H computed using the proposed models, characterizing the microstructure development during the hydration procedure is possible if the physical properties of the products are known.

Brouwers [18, 19, 25] proposed two general models for the composition of C–S–H with different C/S ratios. The influence of C/S ratio on the water content in C–S–H was investigated. Two levels of gel water in C–S–H were proposed, namely constant ''gel'' water and various ''gel'' water. Since until now the water content in C–S–H with various C/S ratios is yet not well known, both models could be valid. Here, the model with the constant ''gel'' water is first used. While the procedures for calculation using the two different models are the same for each other, options of these models yields significantly different results. Later, results using the other model will be compared with those using the constant ''gel'' water model. For the first model, where constant gel water in C–S–H is assumed, the gel porosity of C–S–H is calculated from its composition as [18, 19, 25]:

$$\Phi_{\mathrm{C-S-H}} = \frac{32.44}{94.60 + 33.05(a - 1.7)} \tag{49}$$

Again, incorporating A into C–S–H is assumed not to affect the gel porosity of C–S–H. Substituting a typical value for the C/S ratio of C–S–H from AAS, for example, 1.1, into Eq. (49) yields a porosity of 44.6%. The predicted gel porosity is much higher than the porosity of C–S–H from the hydration of calcium silicate in OPC (33%–38%), having a higher C/S ratio of about 1.7 [18, 19, 25].

According to the classification of Mindess and Young [41], the gel pores mainly comprise those with sizes smaller than 10 nm. Hence, it is reasonable to believe that a large part, probably most, of the gel pores in C–S–H have a size smaller than 10 nm. Considering the large amount of C–S–H in the hardened AAS paste, it would be expected that a large part of pores are gel pores with sizes smaller than 10 nm. This conclusion is also in line with the observations in various researches [31, 39, 42].

Assuming all and only the pores in C–S–H are gel pores and they have the size 0–10 nm, the gel porosity of AAS paste is:

$$\Phi_{\mathrm{gp}} = \frac{V_{\mathrm{C-S-H}} \cdot \Phi_{\mathrm{C-S-H}}}{V_{\mathrm{sl}} + V_{\mathrm{w_0}}} = \frac{n_{\mathrm{C-S-H}} \cdot \omega_{\mathrm{C-S-H}} \cdot \Phi_{\mathrm{C-S-H}}}{m_{\mathrm{sl}}/\rho_{\mathrm{sl}} + \mathrm{w/b} \cdot m_{\mathrm{sl}}/\rho_{\mathrm{w}}} \tag{50}$$

For simplification, among the models proposed in proceeding sections, Model 3 is selected here for the illustration purpose. Thus, practically the moles of C–S–H can be represented by:

$$n_{\mathrm{C-S-H}} = n_{\mathrm{S}} - 2n_{\mathrm{F}} = m_{\mathrm{sl}} \cdot (y_{\mathrm{S}} - 2y_{\mathrm{F}}) \tag{51}$$

Substituting Eq. (51) into Eq. (50) gives:

$$\Phi_{\mathrm{gp}} = \frac{V_{\mathrm{C-S-H}} \cdot \Phi_{\mathrm{C-S-H}}}{V_{\mathrm{sl}} + V_{\mathrm{w_0}}} = \frac{n_{\mathrm{C-S-H}} \cdot \omega_{\mathrm{C-S-H}} \cdot \Phi_{\mathrm{C-S-H}}}{m_{\mathrm{sl}}/\rho_{\mathrm{sl}} + \mathrm{w/b} \cdot m_{\mathrm{sl}}/\rho_{\mathrm{w}}} \tag{52}$$

The capillary pores are considered as those with sizes 10–500 nm [41]. If the sample is cured in the saturated state, water is always available for the hydration. Self-desiccation thus does not take place. All capillary pores are consequences of the chemical shrinkage and the remaining water in the system. Since the hydration proceeds under saturated conditions, extra water can always imbibe, enabling full hydration of the slag. Also, as discussed previously, the chemical shrinkage of the reaction creates internal pores. Hence, the capillary porosity in case of full hydration of slag can thus be calculated as

$$\begin{aligned}\Phi_{\mathrm{cp}} &= \frac{V_{\mathrm{sl}} + V_{\mathrm{w_0}} - V_{\mathrm{hp}}}{V_{\mathrm{sl}} + V_{\mathrm{w_0}}} = \frac{m_{\mathrm{sl}}/\rho_{\mathrm{sl}} + m_{\mathrm{w_0}}/\rho_{\mathrm{w}} - V_{\mathrm{hp}}}{(m_{\mathrm{sl}}/\rho_{\mathrm{sl}} + m_{\mathrm{w_0}}/\rho_{\mathrm{w}})} \\ &= \frac{m_{\mathrm{sl}}/\rho_{\mathrm{sl}} + \mathrm{w/b} \cdot m_{\mathrm{sl}}/\rho_{\mathrm{w}} - V_{\mathrm{hp}}}{(m_{\mathrm{sl}}/\rho_{\mathrm{sl}} + \mathrm{w/b} \cdot m_{\mathrm{sl}}/\rho_{\mathrm{w}})} = 1 - \frac{\rho_0}{m_{\mathrm{sl}}} \sum n_i \cdot \omega_i\end{aligned} \tag{53}$$

in which $\rho_0 = \rho_{\mathrm{sl}} \cdot \rho_{\mathrm{w}} / (\rho_{\mathrm{w}} + \mathrm{w/b} \cdot \rho_{\mathrm{sl}})$, is the density of the initial paste; w/b is the water/binder ratio; V_{w} and $m_{\mathrm{w_0}}$ are the volume and mass of water in the starting paste. The total porosity (sum of gel porosity and capillary) of the paste reads

$$\Phi = \Phi_{\mathrm{cp}} + \Phi_{\mathrm{gp}}. \tag{54}$$

A detailed calculation at the paste level using models proposed in this study yields the phase distribution in the hardened paste on a volume basis (Table 10). In the computation, the slag is assumed to react completely. Slag 1 is taken as example for computation. In the computation, air voids formed due to the initially entrapped air are not taken into account because they might migrate to the surface of the paste due to bleeding. Model 3 is used to model the hydration of slag. The w/b ratio is 0.5.

The models predictions are compared to the measurements in experiments by Collins and Sanjayan [31] (Table 10). The slag used in the experiments has the similar composition as Slag 1. The w/b ratio is also 0.5. But, the samples in the experiments were exposed to 50% RH for up to 56 days. Obvious drying shrinkage was observed during experiments. Hence, the conditions that the paste is subject to in the experiments are not exactly the same as those used in the computation. Furthermore, considering the age of curing, complete reaction of slag can hardly be achieved. However, the results of experiments might still provide valuable clues for the modelling.

C–S–H is shown to be the dominant product in the paste also in a volume basis. Both hydrotalcite and ettringite are formed in significant amounts. The level of the Fe-containing hydrogarnet phase is minor. An important characteristic of the microstructure, the distribution of pores are revealed using the model. In both the prediction and measurements, most pores in AAS paste are shown in the range of gel pores. The predicted pore distribution is further compared to the experimental results by Häkkinen [39], in which it was found most of the pores in AAS mortar are in the range of gel pore and the ratio of gel pores to capillary pores is roughly 2.3. The calculation using the proposed model yields the ratio 2.2. In the studies by Collins and Sanjayan [31] and by Häkkinen [39], the pore size distribution of OPC paste was also measured. Both gave the similar results: for OPC paste, most of the pores were in the range of capillary pores. Therefore, although the C–S–H from AAS hydration has larger gel porosity than the C–S–H from normal OPC hydration, from the viewpoint of the paste, most of the pores in AAS paste exist as gel pores. The capillary porosity of AAS paste is much lower than that of the OPC paste. As capillary pores are generally considered to be responsible for mass and water transfer in the paste, the hardened AAS paste is expected to have good resistance to release or ingression of substances. This can in turn explain the good performance of AAS concrete.

Table 10 Predicted phase distribution in hardened AAS paste and measured porosities

Substance/property	Prediction	Measurement
Product proportion (vol %)		
C–S–H	57.7	–
M_5AH_{13}	16.3	–
$C_6AFS_2H_8$	1.3	–
$C_6A\bar{S}_3H_{32}$	12.8	–
C_4AH_{13}	0	–
C_2ASH_8	0	–
Gel porosity (%)	25.7	19.7
Capillary porosity (%)	11.9	4.5
Total porosity (%)	37.6	24.3

Prediction with Cement 1 and Model 3; w/b = 0.5. Slag has hydrated completely. The capillary pores comprise the unreacted water and the chemical shrinkage. Measurements are taken from Collins and Sanjayan (31)

The total porosity of the paste predicted using the model is significantly higher than the measurement in the experiment. This would be expected because the drying shrinkage of the paste reduces its total porosity. The difference in capillary porosity is more prominent than the gel porosity. The computation of Collins and Sanjayan showed that at 50% RH, almost all the capillary pores are dry while parts of the gel pores are still filled with water. Hence, drying shrinkage can be more severe in capillary pores than in gel pores, which in turn reduces the capillary porosity.

In the other model for C–S–H, namely variable ''gel'' water model, proposed by Brouwers [18, 19, 25], the gel porosity of C–S–H in the saturated state is calculated as:

$$\Phi_{\mathrm{C-S-H}} = \frac{-22.71 + 32.44a}{-16.73 + 65.49a}. \tag{55}$$

Calculation using Eq. (55) and following the same procedure as in the first part of this section yields a comparable total porosity of 34.5%. However, the distribution of the pores is different. The calculated gel porosity amounts to 9.5% and the capillary porosity to 25.0%. In other words, 72% of the pores are in the range of the capillary pore size. This fraction of capillary pore is significantly higher than the measurement in experiments [31, 39, 42]. Hence, for modelling the microstructure of hydrating AAS paste, the model with constant gel water for C–S–H is recommended for future use.

The initial w/b ratio has a dominant influence on the total porosity of the hardened paste because it determines the initial porosity in the system. As the hydration proceeds, these pores will partly or completely be occupied by the hydration products. The total porosity of AAS paste (Slag 1) at full hydration in the saturated

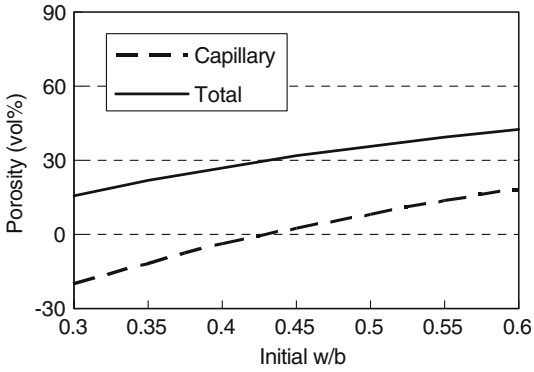

Fig. 3 Relationship between the total porosity, capillary porosity and the initial w/b ratio

state is plotted versus the initial w/b ratio in Fig. 3. With higher initial w/b ratios, the total porosity of the resulting structure is larger. As larger porosity is generally related to lower compressive strength of the resulted paste, the higher w/b ratios would not be preferred when designing a recipe.

However, this cannot be necessarily true if considering the other factors influencing the hydration process of AAS pastes. When a low initial w/b ratio is used, the starting microstructure is more compact, generating a denser barrier for water intrusion while the hydration process proceeds. Thus, as a consequence, the hydration process might progress in a slower rate than pastes with high initial w/b ratios. Furthermore, as shown in the relationship between the initial w/b ratio and the capillary porosity (Fig. 3), if the w/b ratio is lower than a certain value (in the case of Slag 1, roughly 0.4), the capillary porosity is negative, indicating all the initial pores and pores generated by chemical shrinkage are occupied by the hydration products. When this full occupation takes place, further hydration of slag ceases or can only progress at a very low rate. In fact, in the study by Häkkinen [39], slightly swelling of the AAS mortars made with w/b ratio 0.4 was observed while cured under water, which is in line with the predictions in this study. Hence, combined with the conclusion on the water retention by AAS, larger initial w/b ratio (in case of Slag 1, w/b $>$ 0.4) can be preferred with respect to full hydration of slag, but special attention must be paid to the large chemical shrinkage evolved during the hydration process.

Conclusions

Based on investigation in this study, following conclusions can be drawn:

1. The main hydration products in hardened AAS paste include C–S–H, a hydrotalcite phase, a hydrogarnet phase, tetracalcium aluminate hydrate, strätlingite and ettringite. C–S–H is the main hydration product. The quantities of the hydrotalcite, hydrogarnet and ettringite follow from the oxide contents of M, F and $\bar{S}$ in the slag (Eqs. (8)–(10)), respectively.
2. The aluminum from the slag is first combined with the M, F and $\bar{S}$ to form the hydrotalcite, hydrogarnet and ettringite. The remaining A goes into the C–S–H for substituting the S.
3. The A substitution for S in C–S–H is limited to a certain degree structurally related to the C/S ratio as given by Richardson [11] and in Eq. (1). When there is sufficient A from the slag to achieve the maximum substitution degree in C–S–H, the remaining A reacts to the AFm phases (C_4AH_{13} or C_2ASH_8). The formation of the AFm phases more likely occurs with slag high in A and/or low in M.
4. The C/S and A/S ratios in the hydration product C–S–H are different from the C/S and A/S ratios in the starting material (slag). Although C–S–H is the most dominant hydration product, the presence of other products clearly influences its composition.
5. The proposed models can quantify the hydration products of AAS and determine the composition of C–S–H based on the mineral compositions of slags. Predictions of the models are consistent with the experimental observations.
6. With the proposed models, the retained water in the hydration products of AAS can be calculated in different hydration states. Accordingly, the hydration equation can be derived. The hydration of AAS exhibits a higher water demand than the OPC, but in the D-dried state (or being heated to 105 °C), the AAS paste retains less water.
7. In the saturated state, the chemical shrinkage of AAS is significantly higher than that of OPC, which should deserve serious attention in its application.
8. The C–S–H from the AAS hydration has higher gel porosity than C–S–H from the OPC hydration. Most of pores in hardened AAS paste are in the range of gel pores. The AAS paste thus has a finer microstructure than the OPC paste.

Acknowledgements The authors wish to thank the following institutions for their financial support of the present research: Dr. ir. Cornelis Lely Foundation, Delta Marine Consultants, Betoncentrale Twenthe, Rokramix, Dutch Ministry of Infrastructure, SenterNovem Soil+, Jaartsveld Groen en Milieu.

References

1. Glukhovsky VD, Rostovskaja GS, Rumyna GV (1980) In: Proc. 7th ICCC, vol 3, Paris, France, 1980, pp v164–168
2. Narang KC, Chopra SK (1983) Silicates Industrials 9:175
3. Schilling PJ, Roy A, Eaton HC (1994) J Mat Res 9:188
4. Shi CJ, Day RL (1995) Cem Con Res 25:1333
5. Wang SD, Scrivener KL (1995) Cem Con Res 25:561
6. Schneider J, Cincottob MA, Panepuccia H (2001) Cem Con Res 31:993
7. Brough AR, Atkinson A (2002) Cem Con Res 32:865
8. Chen W, Brouwers HJH (2005) J. Mat. Sci. (this issue)
9. Richardson IG, Brough AR, Groves GW, Dobson CM (1994) Cem Con Res 24:813
10. Wang SD, Scrivener KL (2003) Cem Con Res 33:769
11. Richardson IG (1999) Cem Con Res 29:1131
12. Taylor HFW (1997) Cement chemistry, 2nd edn. Thomas Telford, London, UK
13. Harrisson AM, Winter NB, Taylor HFW (1987) Mal Res Soc Symp Proc 85:213
14. Richardson IG, Groves GW (1992) J Mat Sci 27:6204
15. Gollop RS, Taylor HFW (1996b) Cem Con Res 26:1029
16. Locher FW (1960) In: Proc. 4th ICCC, vol 1, Washington D.C., US, 1960, pp 267–276
17. Gollop RS, Taylor HFW (1996a) Cem Con Res 26:1013
18. Brouwers HJH (2003) In: Fisher HB (ed) Proceedings 15th Ibausil (Internationale Baustofftagung), Weimar, 1-0553-1-0566, F.A. Finger-Institut für Baustoffkunde, Weimar, Germany
19. Brouwers HJH (2004) The work of Powers and Brownyard revisited: composition of Portland cement paste, 2nd ed. CE&M Research Report 2004W-006/CME-001, University of Twente, Enschede, The Netherlands
20. Brouwers HJH (2005) Cem Con Res 35:1922
21. Rodger SA, Groves GW (1989) J Am Ceram Soc 72:1037
22. Taylor HFW, Newbury DE (1984) Cem Con Res 14:565
23. Schwiete HE, Ludwig U (1969) In: Proc. 5th ICCC, vol 2, Tokyo, Japan, 1968, pp 37–69
24. Steinour HH (June, 1947) Bull. 18, Res Lab of Portland Cement Association, by American Chemical Society, reprinted from Chem Rev 40(3):391
25. Brouwers HJH (2004) Cem Con Res 34:1697
26. Shimada Y, Yong JF (2001) Adv Cement Concr Res 13:77
27. Allmann VR (1970) Chimia 24:99 (in German)
28. Glasser FP, Kindness A, Stronach SA (1999) Chem Mater 29: 861
29. Wang PZ, Trettin R, Rudert V, Spaniol T (2004) Adv Cem Res 16:1
30. Wassing W (2003) Cement International 5:94
31. Collins F, Sanjayan JG (2000) Cem Con Res 30:1401
32. Song S, Jennings HM (1999) Cem Con Res 29:159
33. Wolhuter CW, Turkstra J, Morris RM (1980) Cem Con Res 10:535
34. Powers TC, Brownyard (1948) Bull 22, Res Lab of Portland Cement Association, Skokie, IL, USA, reprinted from J. Am Concr Inst (Proc.), 43 (1947):101, 249, 469, 549, 669, 845, 933
35. Köster H, Odler I (1986) Cem Con Res 16:207
36. Mills RH (1986) In: Frohnsdorff G (ed) ASTM STP 897, ASTM, Philadelphia, US, pp 49–61
37. Czernin W (1956) Zem-Kalk-Gips 9:525 (in German)
38. Tazawa E, Miyazawa S, Kasai T (1995) Cem Con Res 25:288
39. Häkkinen J (1993) Cem Con Res 23:407
40. Andersson R, Gram HE (1987) Nordic Concr Res 6:7
41. Mindess S, Young JF (1981) Concrete, Prentice-Hall, Englewood Cliffs, NJ, USA
42. Shi CJ (1996) Cem Con Res 26:1789